J Mater Sci
DOI 10.1007/s10853-015-9062-5

Cycling performance and morphological evolution of pulsed laser-deposited FeF_2 thin film cathodes for Li-ion batteries

Shadi Al Khateeb[1] · Aaron G. Lind[2] · Reinaldo Santos-Ortiz[3] · Nigel D. Shepherd[3] · K. S. Jones[2]

Received: 22 December 2014 / Accepted: 27 April 2015

Abstract Electronic conductor-free FeF_2 films deposited by pulsed laser deposition (PLD) were studied as potential cathode materials for Li-ion batteries. The correlation between microstructural evolution and electrochemical cycling of PLD FeF_2 films was investigated. Cross-sectional transmission electron microscopy (X-TEM) of the films indicates that they are composed of particles varying in size between 10 and 50 nm. 20–50 nm particles were initially deposited on the sample substrate and were not cycled, irrespective of film thickness and applied C-rate; 10 nm particles were cycled at low C-rates. Cross-sectional TEM of delithiated films shows that the reconversion process starts from the bottom to the top of the film by forming FeF_2 on the 20–50 nm FeF_2 particles. Galvanostatic measurements show that thinner FeF_2 films have higher capacities and expansion percentages than thick films, but the measured capacity of these films is still less than the theoretical capacity. These results suggest that the cycling performance of PLD FeF_2 is limited by electron transport and that the addition of an electronic conductor will increase the cycling capacity of FeF_2 films.

✉ Shadi Al Khateeb
icytecry@yahoo.com

[1] Department of Materials Engineering, Faculty of Engineering, Al-Balqa' Applied University, Al-Salt 19117, Jordan

[2] Department of Materials Science and Engineering, University of Florida, Gainesville, FL 32611, USA

[3] Department of Materials Science and Engineering, University of North Texas, Denton, TX 76203, USA

Introduction

Pulsed laser deposition (PLD) has been widely used for the deposition of thin films of a variety of materials, such as electrochromic materials (WO_3 [1] and NiO [2]) and battery electrode materials (Co_3O_4 [3], TiS_x [4], and FeF_2 [5]). The use of transition metal fluorides as electrodes in lithium-ion batteries is limited by their poor electronic conductivity due to their large band gap. Improved cycling performance of the electrically insulating iron fluoride has been achieved with the addition of carbon as an electronic conductor for iron fluoride powders [6]. PLD allows for uniform growth of thin films with the electrochemical properties of bulk powders and does not require the addition of binders or electronic conductors required for electrochemical characterization of powders [3, 5]. The PLD technique has been used for the deposition of electronic conductor-free FeF_2 films previously [5, 7, 8], but there are relatively few reports on the use of PLD FeF_2 films as cathodes for Li-ion batteries [5, 7]. FeF_2 is an attractive conversion cathode material due to its high theoretical capacity of 571 mAh/g [5] at full conversion according to Eq. 1:

$$2\ Li^{2+} + \ FeF_2 + \ 2e^- \rightarrow 2\ LiF \ + \ Fe. \qquad (1)$$

The large conversion capacity of FeF_2 gives it a distinct advantage over cathodes of intercalation compounds such as $LiCoO_2$ and $LiFePO_4$, which have capacities ranging from 120 to 200 mAh/g [9–13]. Experimental capacities of PLD FeF_2 films close to the theoretical maximum were obtained using coin cell configuration, and the electrochemical behavior of the FeF_2 films grown at low temperature has been investigated [5, 7]. Studies on the morphological evolution and/or conversion reaction mechanism have been performed on C–FeF_2 powders

Published online: 06 May 2015

prepared by chemical routes [14, 15] and on FeF_2 films prepared by a physical approach [16]. Previous investigations of FeF_2 as a cathode material in lithium-ion cells have resulted in measured capacities ranging from 137 mAh/g to near theoretical capacity with the large range in measured capacities generally being attributed to differences in FeF_2 processing technique or cycling rate (C-rate) [5, 7, 14, 15, 17, 18]. Nevertheless, questions regarding how PLD technique would affect the electronic pathway and morphological evolution during the cycling of electronic conductor-free FeF_2 films deposited by PLD still remain.

We found that the steel components of the coin and pouch cells can contribute to the total capacity of a given cell and result in erroneous capacity measurements; so pouch cells with aluminum leads were used in this work to avoid contributions in capacity from stainless steel components. The effect of film thickness, cycling rate, and the number of cycles on the cycling performance and the corresponding morphological evolution of electronic conductor-free FeF_2 films was investigated.

Experimental

FeF_2 cathode films were deposited via PLD of FeF_2 targets (fabricated from anhydrous FeF_2 powder of 99 % purity: Alfa Aesar) onto 0.5 cm × 0.5 cm × 25 μm AISI 304 stainless steel substrates (Trinity Brand Industries) held at 400 °C at a base pressure of 4–5 × 10^{-7} torr. FeF_2 films were deposited using a 248 nm ultraviolet krypton fluoride excimer laser operated at a frequency of 10 Hz with a fluence of 3.75 J/cm^2 using Lambda Physik, Compex 201.

After PLD deposition onto the stainless steel substrate, test cells were assembled inside a glove box in Ar environment with less than 0.1 ppm H_2O. Figure 1 shows the construction of a pouch cell consisting of Al leads, a 0.75 cm × 0.75 cm × 0.38 mm lithium metal anode (99.9 % purity, Sigma Aldrich), and an 1.5 cm × 1.5 cm × 21.5 μm Celgard C480 polypropylene separator. The FERRO electrolyte solution used in the cells consisted of 1 M $LiPF_6$ in dimethyl carbonate:ethylene carbonate (DMC: EC) (1:1 by volume). The purity of $LiPF_6$ was 99.8 % and the water content of the electrolyte was 20 ppm maximum. In the construction of the pouch cells, the aluminum laminate sheets were heat sealed together to form the body of the pouch. The first heat seal occurred at the leads, which were positioned in a (V) shape. The electrodes were attached to the leads with a piece of Kapton tape. Electrochemical characterization of the assembled cells was performed using galvanostatic and cyclic voltammetry measurements using an Arbin BT2000 over a potential window of 1–4.5 V. Galvanostatic tests were performed at a C-rate of C/1 or C/43, while cyclic voltammetry was performed at 1 mV/s. Herein, C-rate is related to the number of hours required for the cell to charge in the predefined potential window (1–4.5 V), and therefore C/1 denotes a charge rate at which the electrode will be charged from 1 to 4.5 V in 1 h. The samples were coated with 300 nm of amorphous carbon to protect the sample surface from amorphization due the ion beam during the X-TEM lamella formation prior to formation of cross-sectional transmission electron microscopy (X-TEM) sample lamellas using an in situ Focused Ion Beam (FIB: FEI dual-beam Strata DB 235) technique, described elsewhere [19]. All X-TEM sample lamellas after being prepared were immediately transferred from the FIB to the TEM (JOEL 2010F) for structural characterization, and sample exposure to the atmosphere was limited to 3 min or less. Surface structure of the as-deposited films was investigated using a scanning electron microscope (SEM:FEI Dual-Beam Strata DB235).

Results and discussion

Electrochemical measurements

Galvanostatic cycling tests of FeF_2 films of different thicknesses at a constant C-rate of C/1 are shown in Fig. 2. These results indicate that thinner films result in higher measured capacities. A solid electrolyte interface (SEI) formation during first discharge cycle in FeF_2 films has been reported [20], and a capacity in excess of the theoretical value of FeF_2 at C/10 was reported and attributed to the SEI layer formation [5]. The large capacity in the first discharge cycle observed in this work compared to subsequent cycles irrespective of the FeF_2 thickness is also likely due to the formation of an SEI layer.

Discharge–charge curves for the 130 nm FeF_2 film are shown in Fig. 3. These discharge curves are characterized by two sloping voltage regions and indicate that the conversion reaction began at 1.5 V. Such behavior has been observed for PLD FeF_2 films cycled at C/10 [5] and for chemically synthesized FeF_2 powders [15, 18]. The first sloping region shown in Fig. 3 accounts for up to 20 mAh/g, and it was reported that such sloping is due to the formation of SEI and the involvement of both intercalation and conversion in early stages of the discharge [18, 21]. A second sloping region starts at the discharge potential of 1.5 V. Sloping has been observed in previous studies of FeF_2 films [5] and powders [15, 18], but the cause has not been identified and requires future investigation.

The cyclic voltammetry tests of different film thicknesses shown in Fig. 4 indicate that the conversion (discharge) reaction occurs at larger peak currents for the thinner films, which suggests that inefficient conversion is

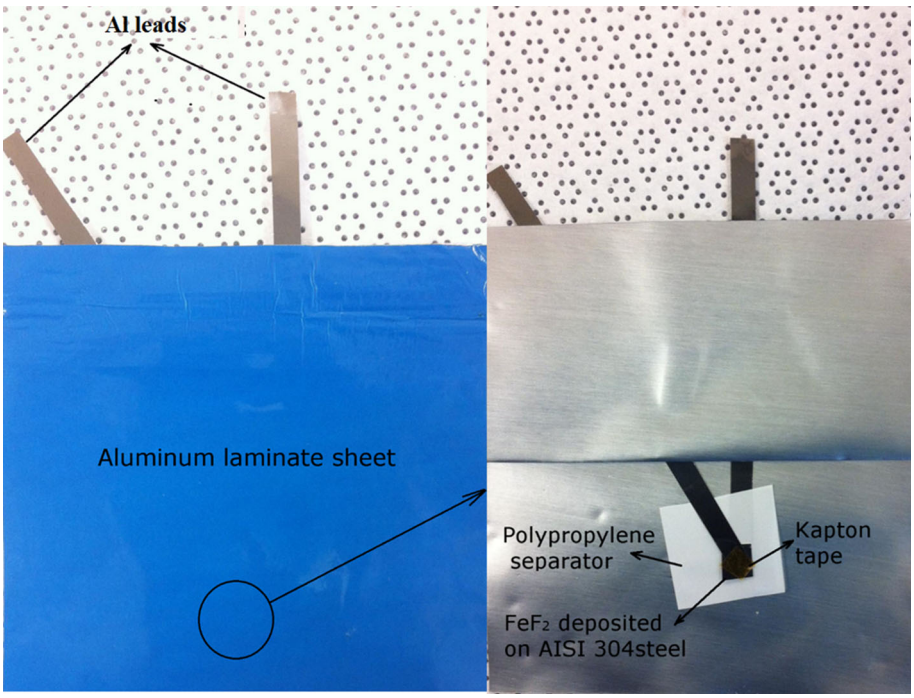

Fig. 1 Pouch cell battery showing the different components and cell construction

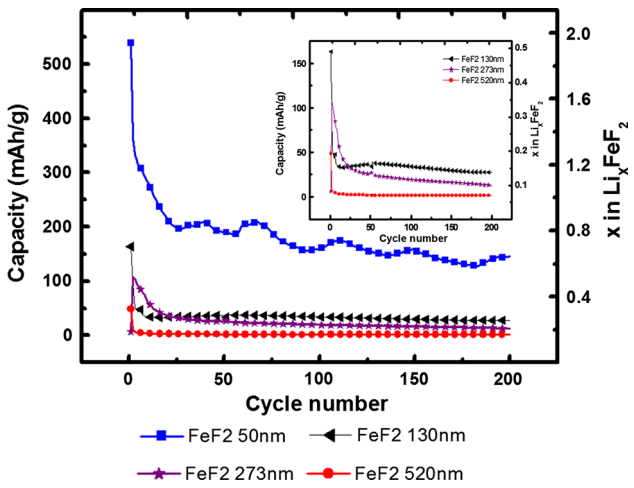

Fig. 2 Galvanostatic test of the FeF_2 films showing the discharge capacity as a function of cycle number and films' thicknesses using pouch cells with aluminum leads. The films were cycled at a C-rate of C/1. The *inset* shows a closer view on the capacities of 130, 273, and 520 nm films

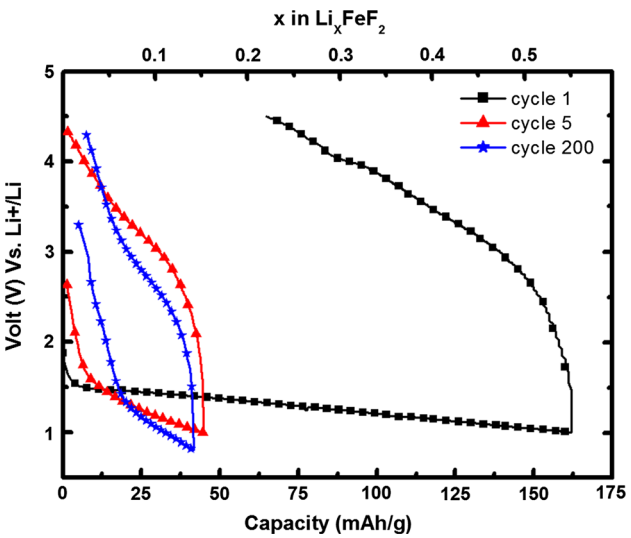

Fig. 3 Discharge–charge curves for the 130 nm FeF_2 film using pouch cell with aluminum leads cycled in a voltage window of 1–4.5 V at a C-rate of C/1

occurring in thicker films and lower capacities are consequently obtained as observed in Fig. 2. Larger peak currents in the thinner films are due to more efficient conversion of FeF_2, which may indicate that conversion is limited by either electrolyte access (diffusion limited) or electron transport. Charging peaks between 2.75 and 3.25 V were also observed, similar to those reported for C–FeF_2 prepared by a chemical approach and cycled at different C-rates [14, 15, 18]. During the first charge cycle for the FeF_2 films (Fig. 4), two resolved peaks were observed. The first peak was observed at approximately 3.2 V, and the second peak was detected at 3.9 V. On subsequent charge cycles, only the peak at 3.2 V was detected as shown for an 80 nm film (Fig. 5b). Similar peaks were observed by other researchers for $LiPF_6$ stabilized with tris(2,2,2-trifluoroethyl) phosphite, where a peak at about 4 V appeared due to an electrolyte reaction during the charging cycle of Li/graphite and Li/cathode half-cells

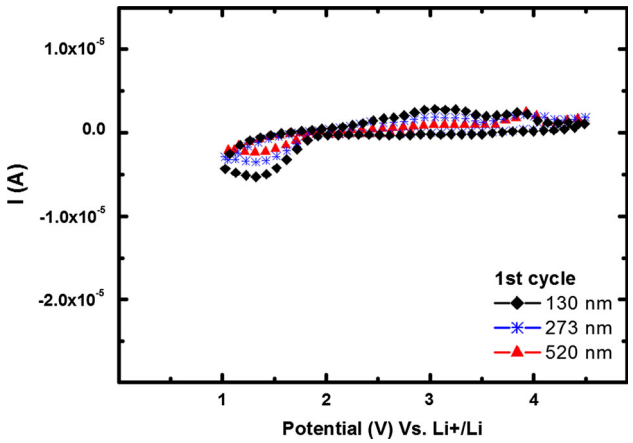

Fig. 4 Cyclic voltammogram of the first discharge of FeF_2 films at different thicknesses using pouch cells with aluminum leads cycled in a potential window of 1–4.5 V at a scan rate of 1 mV/s

[22]. $LiPF_6$ (1 M) in 1:1:1 ethylene carbonate/diethyl carbonate/dimethyl carbonate(EC/DEC/DMC) electrolyte has also been observed to decompose at 4.8 or 5.2 V, versus lithium metal on a glassy carbon electrode depending on the additives in the electrolyte [23]. A peak at 3.9–4.2 V was detected for FeF_3 nanowires in the first charge cycle, which was attributed to electrolyte oxidation [24]. For FeF_2/C films prepared by hydrothermal synthesis [17], a peak at 4.3 V was detected during the charging of the film using coin cells, but the cause of this peak was unidentified. SEI formation during the first discharge cycle of FeF_2 films was reported to be the cause of the large first cycle capacity [5, 20]. SEI formation is the most likely explanation for the peak at 3.9 V in this work, given that the peak at 3.9 V was only observed on the first cycle of the films (Fig. 5b).

The 80 nm films were discharged at a slower C-rate (C/43) in an attempt to increase the capacity of the cycled FeF_2 films. As the capacity of the thicker films in Fig. 2 was found to stabilize after 25 cycles, the 80 nm film was cycled for 50 cycles. The discharge capacity of the film after the 50th lithiation cycle was 324 mAh/g (Fig. 5a). This large capacity agreed with a larger discharge peak current (Fig. 5b) per mass compared to those of the thicker films shown in Fig. 4. Similar sensitivity of the discharge capacity to C-rate was also reported for FeF_2 powders where larger capacities were reported at slower discharge rates, and this behavior was attributed to the sluggish kinetics of the conversion process [18]. It can be seen in Fig. 5a that the conversion potential of 1.55 V obtained from the galvanostatic test matches the results from the cyclic voltammetry test shown in Fig. 5b. The conversion potential of the 80 nm films is almost the same as that obtained for the 130 nm FeF_2 film (1.5 V in Fig. 3) at C/1, which agrees well with the reported conversion potential trend for FeF_2 powders [18], but no microstructural investigation relating the effect of C-rate to the obtained capacity of a PLD electronic conductor-free FeF_2 film was performed in the previous studies. The low capacities obtained in Figs. 3 and 5a relative to the theoretical value of 571 mAh/g indicate that the conversion process becomes less efficient with increasing cycling rate and increasing thickness. The inefficient or incomplete conversion might be due to limited electron transport (as FeF_2 is insulating in nature [25]) or a restricted access of the electrolyte to the FeF_2 (diffusion limited), which are subsequently discussed in "Morphological evolution" section.

Morphological evolution

X-TEM samples were used to observe the microstructural evolution of PLD FeF_2 films during cycling. Figure 6a shows the 130-nm-thick as-deposited polycrystalline film that was observed following PLD of FeF_2 onto stainless steel substrates, while Fig. 6b shows the selected area electron diffraction (SAED) confirming the polycrystalline nature of the PLD film in the as-deposited state. FeF_2 peaks were identified based on the d-spacing of the standard JCPDS file 01-071-1968; however, diffraction peaks from

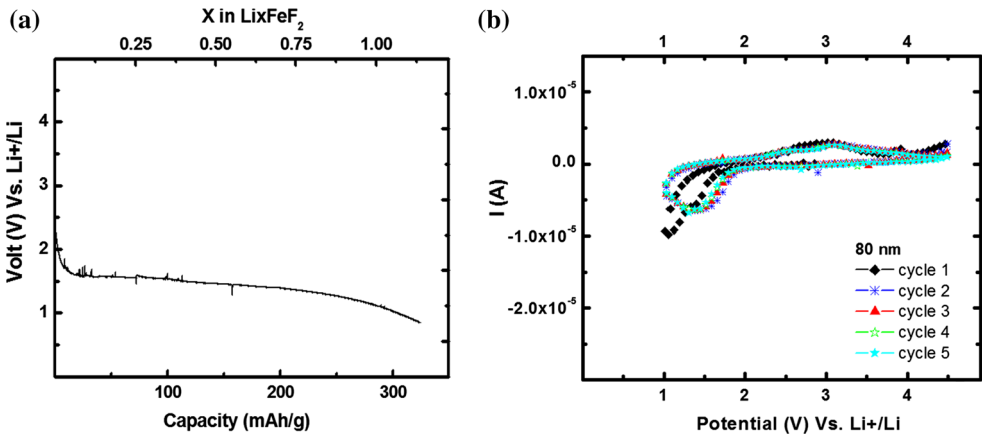

Fig. 5 The cycling of the 80 nm FeF_2 film using pouch cells with aluminum leads. **a** Galvanostatic test at a C-rate of C/43 showing the discharge curve in a voltage window of 1–4.5 V and **b** cyclic voltammogram in a potential window of 1–4.5 V at a scan rate of 1 mV/s

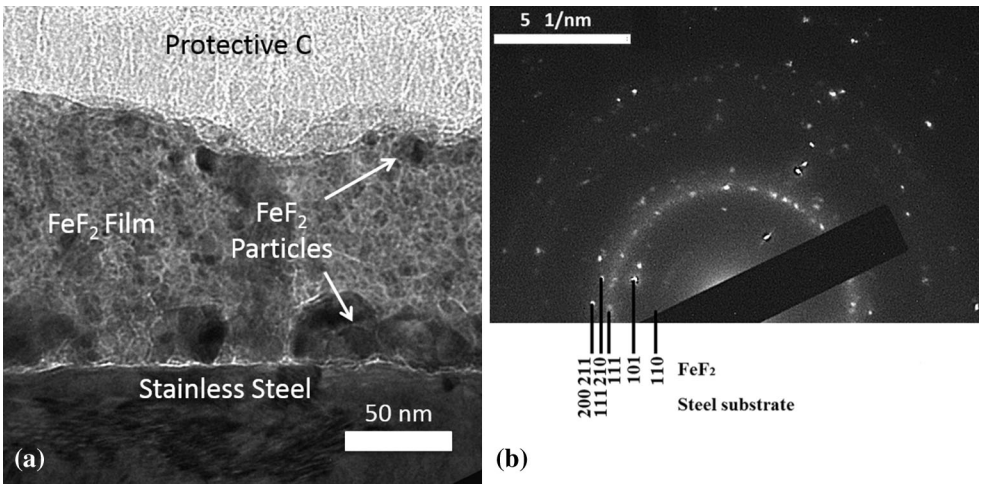

Fig. 6 **a** Bright-field TEM image of the as-deposited 130 nm FeF_2 film showing FeF_2 particles at the substrate surface with a size of 20–50 nm and particles dispersed in the film with a size of 10–20 nm and **b** the corresponding selected area electron diffraction pattern

the AISI 304 substrate were also detected and identified by d-spacing comparison with the standard JCPDS files 00-033-0397. Figure 6a indicates that PLD generated a range of particles from 10 to 50 nm, with particles near the substrate consisting of mostly 20–50-nm-diameter particles; these formed a layer at the substrate surface with an average thickness of 30 nm, and particles within the FeF_2 film were generally finer, in the 10–20 nm range. Figure 7a, b shows the microstructure of discharged (lithiated) 130 nm FeF_2 films, while Fig. 7c, d shows the charged (delithiated) films after 1 cycle and 200 cycles, respectively. Comparison of the post-cycling microstructure at a C-rate of C/1 after 1 and 200 cycles indicates that an incomplete conversion of the film took place during cycling. Incomplete cycling of these films is apparent based on the difference in microstructure with the as-deposited film shown in Fig. 6 and agrees with the low capacity observed in galvanostatic tests shown in Fig. 2. TEM of lithiated films after 1 cycle and 200 cycles, shown in Fig. 7a, b, respectively, also shows incomplete conversion, as evidenced by the large FeF_2 particles near the interface of the current collector and the small FeF_2 particles in the deposited film. Incomplete conversion of the film in Fig. 7b is also confirmed by the presence of LiF and Fe in addition to FeF_2 in the selected area diffraction of these films shown in Fig. 8. The presence of LiF and Fe was detected and identified according to the d-spacings of the standard JCPDS 01-071-1968, 00-045-1460, and 00-001-1252. Due to low scattering factor and low crystallinity of the LiF [10], there is an overlap between the LiF peaks and those of FeF_2 and Fe, which has been observed by others [16].

The conversion reaction of FeF_2 is accompanied by a volumetric expansion, which is an interesting subject for future investigation; however, in this work film expansion along the film thickness will be discussed. The expansion observed in the 130 nm films was calculated based on the post-deposition and post-cycling film thicknesses in Figs. 6a and 7, assuming that the first 30 nm of un-cycled FeF_2 as observed by TEM had no contribution to overall expansion of the films as a result of the conversion reaction. This assumption results in a measured expansion of the active layer from 100 nm to 111 nm for the lithiated film after one cycle (Fig. 7a), resulting in a total expansion of 11 %. Galvanostatic testing of the 130-nm-thick FeF_2 film resulted in a measured capacity plateau of 45 mAh/g (Fig. 2), and when the capacity is corrected to reflect the cycling of only the first 100 nm, a capacity of 55 mAh/g is achieved, assuming a linear relationship between the capacity and thickness as seen in the inset of Fig. 2. The corrected capacity is only 9.6 % of the 571 mAh/g theoretical capacity of FeF_2. The first cycle capacity of the 130 nm film was 162 mAh/g (Fig. 2). Correcting for the 100 nm film results in a capacity of 200 mAh/g, which represents 35 % of the theoretical capacity. The large capacity difference between the 1st cycle and the 200th cycle may further confirm that the large capacity in the first cycle and the peaks at 3.9 V in Figs. 4 and 5 were not due to the film cycling but to the SEI formation. The expansion percentage of the 130 nm film lithiated after the 200th cycle was about 15 %, which is similar to the 11 % expansion in the cycled layer measured for the lithiated film after one cycle. Some variation in the expansion percentage might be due to slight thickness variations in the as-deposited FeF_2 films used for each of the two samples, as TEM of the as-deposited films in Fig. 6 indicates that the films are not completely uniform. It can be concluded that the number of cycles had little effect on the obtained capacity and the large capacity of the first cycle was likely due to the

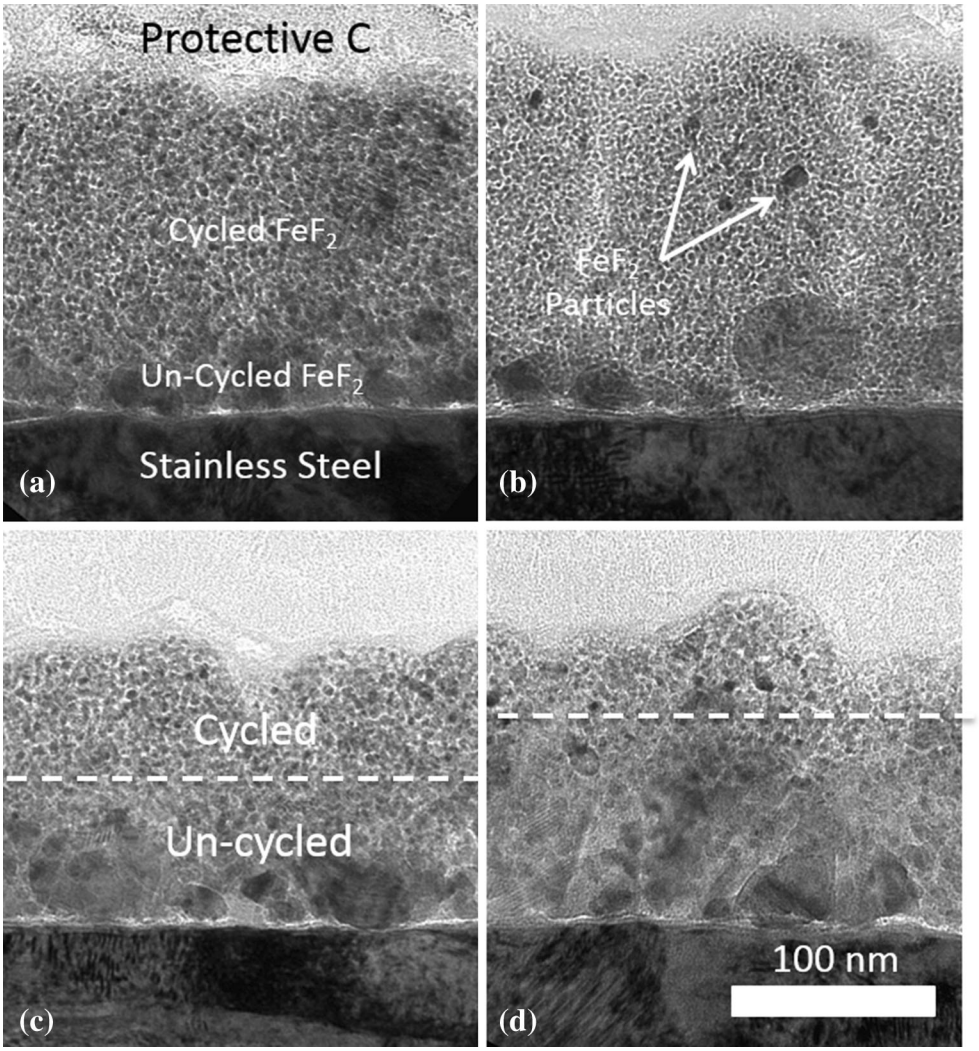

Fig. 7 Bright-field TEM images of the 130 nm FeF_2 film after galvanostatic cycling at C/1 using pouch cells with aluminum leads after lithiation for **a** one cycle showing a thickness of 141 nm and **b** two hundred cycles showing a thickness of 145 nm and after delithiation for **c** one cycle showing a thickness of 133.8 nm and **d** two hundred cycles showing a thickness of 139 nm

formation of SEI, as observed from the similar microstructural evolution as a function of number of cycles (Fig. 7a, b), and nearly constant capacity of the 130 nm film over a large number of cycles (Fig. 2). X-TEM of the 130 nm FeF_2 films after being charged (delithiated) for 1 and 200 cycles is shown in Fig. 7c, d, respectively. Two regions were identified for these films: the upper cycled region and the lower un-cycled region. The microstructure of the cycled region resembles the lithiated film depicted in Fig. 7a, b, whereas the un-cycled region resembles the microstructure of the as-deposited FeF_2 film depicted in Fig. 6a. The cycled region of the 130-nm-thick FeF_2 in Fig. 7c was found to be 60 nm thick, and 73.8-nm of the FeF_2 remained un-cycled. The total thickness of 133.8 nm resulted in a measured expansion of 3.8 % after delithiation compared to the thickness of the as-deposited FeF_2 film (130 nm). The thickness of the FeF_2 film should return back to 130 nm upon full delithiation; however, the 3.8 % expansion remained in the film after the delithiation process, confirming incomplete delithiation. It is mentioned earlier that the thickness of the active film is 100 nm, but after the first delithiation cycle (Fig. 7c), the thickness of the active material became 73.8 nm (un-cycled region).Thinner films result in larger capacities, as seen in Fig. 2. Thinner layers of active material may explain the slight increase in the capacity observed after the first few cycles for the 130 nm film. The larger thickness of the un-cycled region (73.8 nm) (Fig. 7c), compared to 30 nm of FeF_2 in the lithiated film shown in Fig. 7a, suggests that during the delithiation process FeF_2 started to reform by building up through diffusion on the already-existing FeF_2 particles at the substrate surface further indicating that the

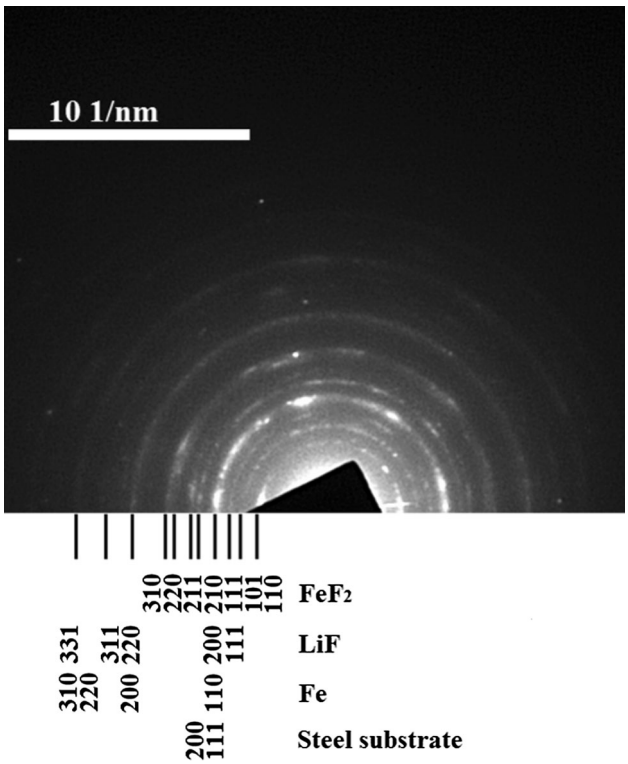

Fig. 8 Selected area electron diffraction (SAED) of the lithiated FeF_2 film after 200 cycles shown in Fig. 7b

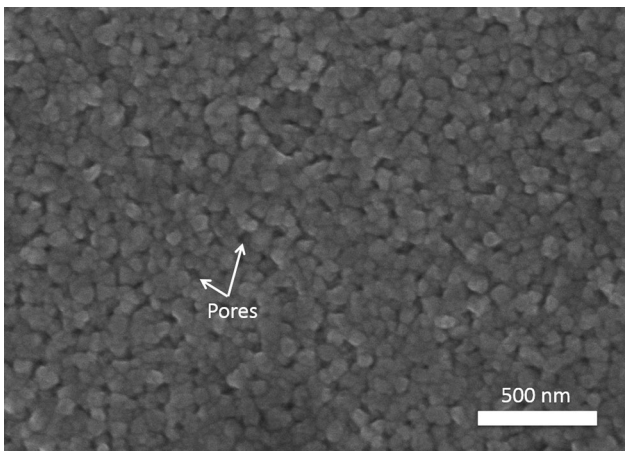

Fig. 9 SEM image showing the porous nature of the as-deposited 130 nm FeF_2 film

delithiation process started from the bottom towards the top of the film. The delithiation process might be explained by the following process: porosity improves ionic transport and hence the amount of film in contact with the electrolyte. The porosity in the as-deposited 130 nm FeF_2 as evidenced by the SEM image in Fig. 9, which might also be an interconnected porous structure, may cause the entrapment of the electrolyte, subsequently facilitating the delithiation of FeF_2 particles at the substrate surface. Further characterization of the porous nature of the FeF_2 films is required using scanning probe microscopy for porosity quantification. The TEM images of the delithiated samples in Fig. 7c, d shows that the structure of the top part of the film is similar to the lithiated samples in Fig. 7a, b, suggesting that lithiated films were not totally reconverted back from (LiF and Fe) into FeF_2. Incomplete reconversion was less pronounced after the 200th charge cycle (Fig. 7d), where the thickness of the cycled (lithiated) region was 37 nm compared to 60 nm after the first charge cycle. The incomplete reconversion of FeF_2 from the current collectors toward the film surface resulted in thicker reformed FeF_2 (or thinner lithiated) films after 200 cycles relative to one cycle and indicates that the restricted access of the electrolyte (diffusion limited) was not the limiting factor in the conversion–reconversion cycles of the PLD electronic conductor-free FeF_2 films. As such, electron transport is more likely to be the factor that controls and limits the amount of FeF_2 involved in the conversion–reconversion reactions since it is expected that if the conversion–reconversion process was diffusion controlled, the thickness of the cycled (lithiated) regions in Fig. 7c, d should be independent of the number of cycles.

In addition to the presence of large (20–50 nm) FeF_2 particles at the substrate surface, which are present before and after the cycling, small dispersed FeF_2 particles of 10–20 nm were also present in the film before and after the cycling (compare Figs. 6a, 7). Neither of these particles was observed to be involved in the conversion–reconversion reaction at the fast C-rate (C/1), which further contributed to the low capacity observed in the galvanostatic tests in Fig. 2. An 80 nm film was discharged at C/43 in an attempt to cycle the FeF_2 particles at the substrate surface and the dispersed particles in the film. It is obvious from the TEM image of the 80 nm film after 50 cycles shown in Fig. 10 that this 80 nm film still has a 30 nm layer of FeF_2 particles at the substrate surface, which are not involved in the conversion reaction. The active film shows an expansion percentage after the 50th lithiation cycle of 84 %. If the capacity in Fig. 5a is corrected for a 50 nm active film, then the capacity would be 446 mAh/g, which represents 78 % of the theoretical capacity. Accordingly, there is 1.56 Li uptake upon cycling at C/43 during the conversion reaction as seen in Eq. 2 compared to 0.15 Li for the 130 nm film cycled at C/1. The micrograph of the post-cycling morphology of the 80 nm film cycled at C/43, shown in Fig. 10, indicates that the small (10–20 nm) FeF_2 particles were no longer present after cycling when a lower C-rate was used, but large particles near the current collector interface still show the presence of un-cycled FeF_2. The galvanostatic testing of the 80 nm film cycled at C/43 indicates that the use of a slow C-rate together with a

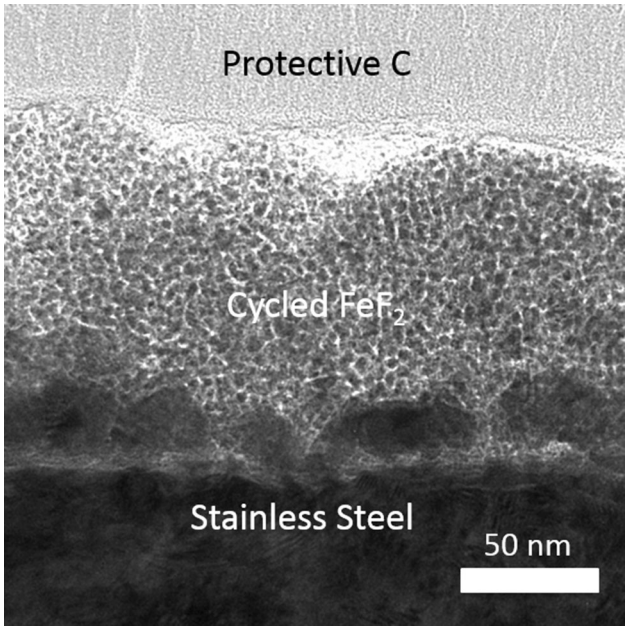

Fig. 10 Bright-field TEM image of the 80-nm-thick as-deposited FeF_2 film after the 50th lithiation cycle at C/43 using pouch cells with Al leads. The total cathode film thickness after cycling was measured to be 122 nm

thinner film would cycle the small, dispersed particles and lead to larger capacities closer to the theoretical maximum.

$$1.56\ Li^{2+} + 0.78\ FeF_2 \rightarrow 1.56\ LiF + 0.78\ Fe \quad (2)$$

The results discussed here suggest that the restricted access of electrolyte to the cathode during the conversion–reconversion cycles is not the capacity-controlling factor in these films. Electron-limited transport is more likely to result in the observed capacity limits, given the following observations. The delithiated film after one cycle has a larger un-reconverted film (cycled region) compared to the one after 200 cycles (Fig. 7c, d, respectively), and there is a larger expansion percentage after the lithiation cycles for the 80 nm film (Fig. 10) compared to the 130 nm film (Fig. 7b); and capacities much lower than the theoretical were obtained even when cycling the FeF_2 film at slow C-rate (C/43).

Conclusions

It was found that capacity increased by decreasing the thickness of the deposited FeF_2 films and agreed with the increase in the discharge peak current as seen from the cyclic voltammetry test. The slower the C-rate and the thinner the FeF_2 films, the larger the Li uptakes. The conversion–reconversion reaction was controlled by the slow access of the electrolyte (diffusion limited) into the FeF_2 films and the slow electron transport, which was probably the dominant over the diffusion.

It was reported that the thin film deposition technique has the benefit over the powder technique and that no binder or electronic conductors are required for subsequent electrochemical characterization [3, 5]. However, the results of this work suggest that complete conversion of PLD FeF_2 cathodes is more likely to be achieved with the deposition of an electronic conductor (such as carbon). This would improve the conductivity of the films and subsequently ease the conversion of FeF_2, resulting in capacities closer to the theoretical maximum upon cycling. Further improvements could come from controlling the deposition parameters to eliminate the large FeF_2 particles that formed in the early stages of deposition on the substrate surface, as these were not shown to contribute to overall cell capacity.

Acknowledgements The corresponding author acknowledges the Scientific Research Support Fund (SRSF), Jordan, for supporting this work performed at the University of Florida.

References

1. Rougier A, Portemer F, Quédé A, El Marssi M (1999) Characterization of pulsed laser deposited WO_3 thin films for electrochromic devices. Appl Surf Sci 153:1–9. doi:10.1016/S0169-4332(99)00335-9
2. Bouessay I, Rougier A, Poizot P, Moscovici J, Michalowicz A, Tarascon JM (2005) Electrochromic degradation in nickel oxide thin film: a self-discharge and dissolution phenomenon. Electrochim Acta 50:3737–3745. doi:10.1016/j.electacta.2005.01.020
3. Pralong V, Leriche JB, Beaudoin B, Naudin E, Morcrette M, Tarascon JM (2004) Electrochemical study of nanometer Co_3O_4 Co, $CoSb_3$ and Sb thin films toward lithium. Solid State Ion. 166:295–305. doi:10.1016/j.ssi.2003.11.018
4. Matsuyama T, Sakuda A, Hayashi A, Togawa Y, Mori S, Tatsumisago M (2012) Preparation of amorphous TiS x thin film electrodes by the PLD method and their application to all-solid-state lithium secondary batteries. J Mater Sci 47:6601–6606. doi:10.1007/s10853-012-6594-9
5. Makimura Y, Rougier A, Tarascon J-M (2006) Pulsed laser deposited iron fluoride thin films for lithium-ion batteries. Appl Surf Sci 252:4587–4592. doi:10.1016/j.apsusc.2005.06.043
6. Badway F, Pereira N, Cosandey F, Amatucci GG (2003) Carbon-metal fluoride nanocomposites: structure and electrochemistry of FeF_3: C. J Electrochem Soc 150:A1209–A1218. doi:10.1149/1.1596162
7. Makimura Y, Rougier A, Laffont L et al (2006) Electrochemical behaviour of low temperature grown iron fluoride thin films. Electrochem Commun 8:1769–1774. doi:10.1016/j.elecom.2006.08.004
8. Santos-Ortiz R, Volkov V, Schmid S et al (2013) Microstructure and electronic band structure of pulsed laser deposited iron fluoride thin film for battery electrodes. ACS Appl Mater Interfaces 5:2387–2391. doi:10.1021/am3017569
9. Ellis BL, Lee KT, Nazar LF (2010) Positive electrode materials for Li-ion and Li-batteries. Chem Mater 22:691–714. doi:10.1021/cm902696j
10. Sina M, Nam KW, Su D et al (2013) Structural phase transformation and Fe valence evolution in FeO_xF_{2-x}/C nanocomposite

electrodes during lithiation and de-lithiation processes. J Mater Chem A 1:11629–11640. doi:10.1039/c3ta12109g
11. Goodenough JB, Kim Y (2009) Challenges for rechargeable Li batteries. Chem Mater 22:587–603. doi:10.1021/cm901452z
12. Xiang H, Zhang D, Jin Y, Chen C, Wu J, Wang H (2011) Hydrothermal synthesis of ultra-thin $LiFePO_4$ platelets for Li-ion batteries. J Mater Sci 46:4906–4912. doi:10.1007/s10853-011-5403-1
13. Li J, Zhao R, He X, Liu H (2009) Preparation of $LiCoO_2$ cathode materials from spent lithium–ion batteries. Ionics 15:111–113. doi:10.1007/s11581-008-0238-8
14. Wang F, Robert R, Chernova NA et al (2011) Conversion reaction mechanisms in lithium ion batteries: study of the binary metal fluoride electrodes. J Am Chem Soc 133:18828–18836. doi:10.1021/ja206268a
15. Reddy MA, Breitung B, Chakravadhanula VSK et al (2013) CF_x derived carbon–FeF_2 nanocomposites for reversible lithium storage. Adv Energy Mater 3:308–313. doi:10.1002/aenm.201200788
16. Rangan S, Thorpe R, Bartynski RA et al (2012) Conversion reaction of FeF_2 thin films upon exposure to atomic lithium. J Phys Chem C 116:10498–10503. doi:10.1021/jp300669d
17. Bai Y, L-w Yang F Wu et al (2013) High performance FeF_x/C composites as cathode materials for lithium-ion batteries. J Renew Sustain Energy 5(021402):021401–021409. doi:10.1063/1.4798423
18. Armstrong MJ, Panneerselvam A, O'Regan C, Morris MA, Holmes JD (2013) Supercritical-fluid synthesis of FeF_2 and CoF_2 Li-ion conversion materials. J Mater Chem A 1:10667–10676. doi:10.1039/c3ta12436c
19. Giannuzzia LA, Stevieb FA (1999) A review of focused ion beam milling techniques for TEM specimen preparation. Micron 30:197–204. doi:10.1016/S0968-4328(99)00005-0
20. Boyd S, Amatucci G, Pereira N, Greenbaum S (2013) Solid electrolyte interphase formation in iron (II) fluoride conversion electrodes. 224th ESC Meeting MA2013-02, pp 933–933
21. Yamakawa N, Jiang M, Key B, Grey CP (2009) Identifying the local structures formed during lithiation of the conversion material, iron fluoride, in a Li ion battery: a solid-state NMR, X-ray diffraction, and pair distribution function analysis study. J Am Chem Soc 131:10525–10536. doi:10.1021/ja902639w
22. Zhang SS, Xu K, Jow TR (2002) A thermal stabilizer for $LiPF_6$-based electrolytes of Li-ion cells. Electrochem Solid State Lett 5:A206–A208. doi:10.1149/1.1499669
23. Yang L, Lucht BL (2009) Inhibition of electrolyte oxidation in lithium ion batteries with electrolyte additives. Electrochem Solid State Lett 12:A229–A231. doi:10.1149/1.3238486
24. Li L, Meng F, Jin S (2012) High-capacity lithium-ion battery conversion cathodes based on iron fluoride nanowires and insights into the conversion mechanism. Nano Lett 12:6030–6037. doi:10.1021/nl303630p
25. Qiu SR, Yarmoff JA (2001) Self-limiting growth of transition-metal fluoride films from the reaction with XeF_2. Phys Rev B 63:1154091–1154097